CHAPTER V

MAGNETICALLY CONTROLLED TECHNIQUE FOR ANTENNA BEAM PATTERN RECONFIGURATION

5.1 Introduction

Unlike the conventional pattern reconfiguring techniques, fluidic channels show a linear response, has conformability for any shape and is resilience to wear and tear [1, 2]. Liquid materials have been mostly used to alter the antenna operating frequency [2-8]. There are, however, few reports where fluidic channels have been used either as parasitic elements or as tuning elements for planar antennas, to steer the beam, [1, 9-12], and mostly mechanically pumped fluids are used as a switching mechanism.

The fluidic actuator proposed in this chapter exploits the conductive property of the liquid for beam steering. Here, two immiscible fluids of different conductivity are injected in a microchannel to form the directing element. The directing elements are placed across the corners of a standard rectangular microstrip patch antenna. The design of the structure is kept similar to that studied in Chapter III, this will also give a comparison to the performance of fluidic actuator with the PIN diode switching for reconfigurability. One of the fluid in the microchannel is magnetic in nature. The relative positions of the two liquids inside the channels are proximity controlled by electromagnets. The work presented is sequenced as design of microfluidic actuated directing element, antenna structural design and performance study.

5.2 Design of microfluidic directing element

Selection of fluids and construction of the microfluidic element

The electrical conductivity of the liquid used in the proposed microfluidic system plays an important role to form antenna's directing elements. The two liquids in the channels should have sufficient conductivity variance and should be immiscible. The magnetic fluid is non-polar, low conducting constituent of the immiscible fluidic system. The other fluid is a polar liquid with relatively higher conductivity. The magnetic fluid also known as ferrofluid (FF) is a colloidal dispersion of small single-domain magnetite nanoparticles in a hydrocarbon based carrier fluid (hexane). FF is synthesized as per the procedures discussed in Chapter IV. A 10 molar solution of NaCl prepared in deionized water is used as the high

conductivity polar fluid. In addition, the solution also provides a slip layer between the FF and the channel wall which helps in reducing the wettability of the magnetic suspension. The electrical conductivity of both ferrofluid and NaCl solution is measured using Merck Inolab Cond 7110 conductivity meter and it is found 0.4 S/m and 30 S/m, respectively.

The microfluidic channel used as the directing elements is made up of Polytetrafluoroethylene (PTFE) microchannel of diameter ~ 0.8 mm and wall thickness of 0.1 mm. The two liquids are injected into the channel and the section of the channel occupied by the conductive liquid will serve as the directing element. The length of the channel occupied by NaCl, L_{NaCl} is kept equal to the length of the antenna patch, L in accordance with the criterion given for the Yagi formation [13]. While the FF occupies a length, L_{FF} = 2.00 mm. Details of the fluidic antenna element is shown in Figure 5.1.

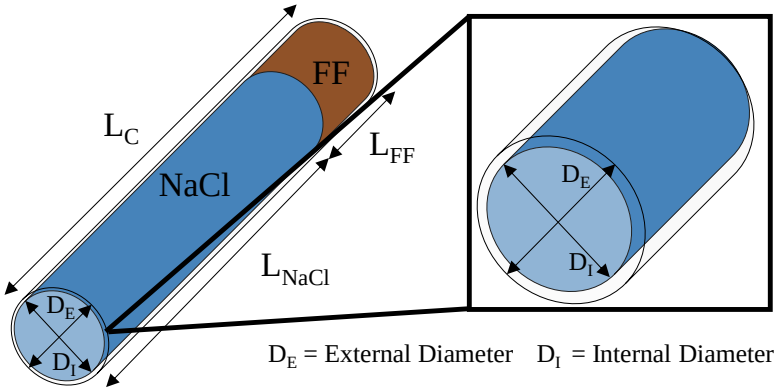

Figure 5.1 Schematic diagram of the constructed microfluidic channel. L_C = 10.38 mm, D_E = 0.9 mm, D_I = 0.8 mm, L_{NaCl} = 8.38 mm and L_{FF} = 2.00 mm

Actuation mechanism

The position of the non-conducting magnetic colloidal dispersion (FF) is controlled using a contactless mechanism consisting of two electromagnets (EM). Initially, FF is positioned at the far end of the channel and the conductive NaCl solution has the required length to be a directing element. Moving the insulating solution from its initial position to the middle part of the channel, splits the conductive solution into two smaller parts. This eventually deactivates the channel functionality as

director, as the shortened length of each individual parts < 0.8L. The working of the switching mechanism is illustrated in Figure 5.2.

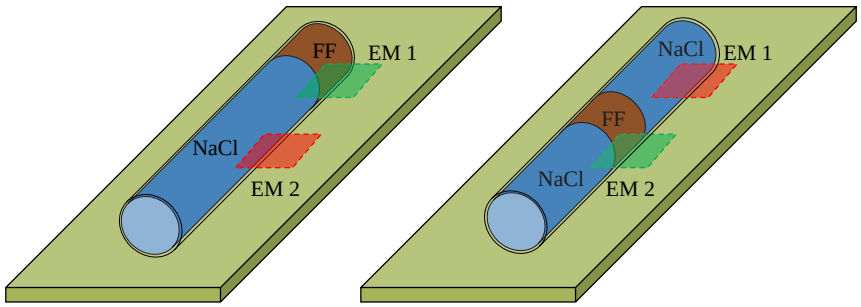

(a) (b)

Figure 5.2 Proposed actuation mechanism of microfluidic channel. In (a) EM 1 is ON, EM 2 is OFF and FF is positioned at the far end, while in (b) EM 2 is ON, EM 1 is OFF and FF is shifted to the middle of the channel

5.3 Design of beam reconfigurable antenna using microfluidic switch

The proposed antenna is a combination of rectangular microstrip patch antenna and Yagi antenna in planar form. It has two parts, one driven element and four sets of parasitic elements.

5.3.1 Driven Element

The driven element is a basic rectangular microstrip patch, with dimension calculated using the TLM equations [14]. The patch is designed to resonate at 8.00 GHz on an FR4 substrate of thickness 1.6 mm and dielectric constant 4.3. The patch is edge fed by a microstrip line with a quarter wave transformer attached. The driven element is made up of solid copper sheet of thickness 0.03 mm.

5.3.2 Parasitic elements

The designed reconfigurable antenna elements are placed across the driven element as shown in Figure 5.3. The elements are arranged in four sets. The fluidic channel is pasted on the substrate rather than embedded as this may change the effective permittivity of the substrate, leading to a shift in the resonant frequency.

X and Y axis position optimization of directing element

The positions of the directing elements with respect to the driving antenna patch are optimized to get the same level of beam shift along all the possible directions.

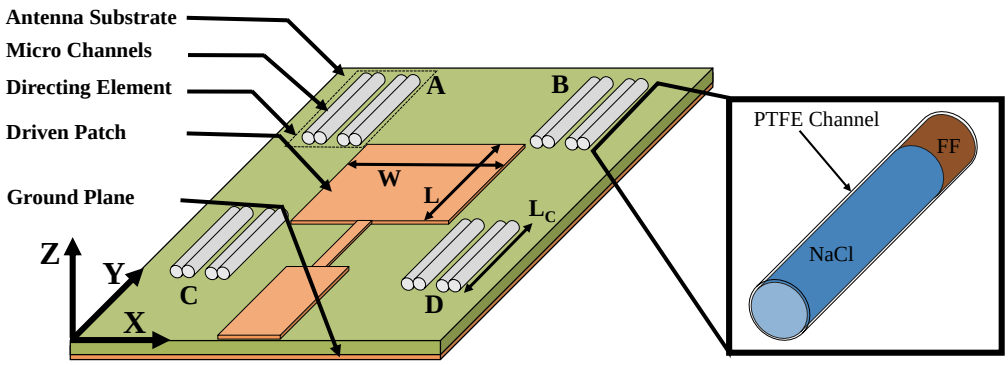

Figure 5.3 Schematic diagram of the proposed antenna showing the constituent elements

The symmetrical geometry of the edge-fed RMP antenna is of special interest in this regard. The designed driving patch antenna, without the directing elements, has a mirror plane symmetry across the feed line. To get the desired uniformity in the extent of shifting from the initial broadside pattern, the positions of the tubes w.r.t. the driving element are first adjusted for one side of the antenna and then replicated to the other plane.

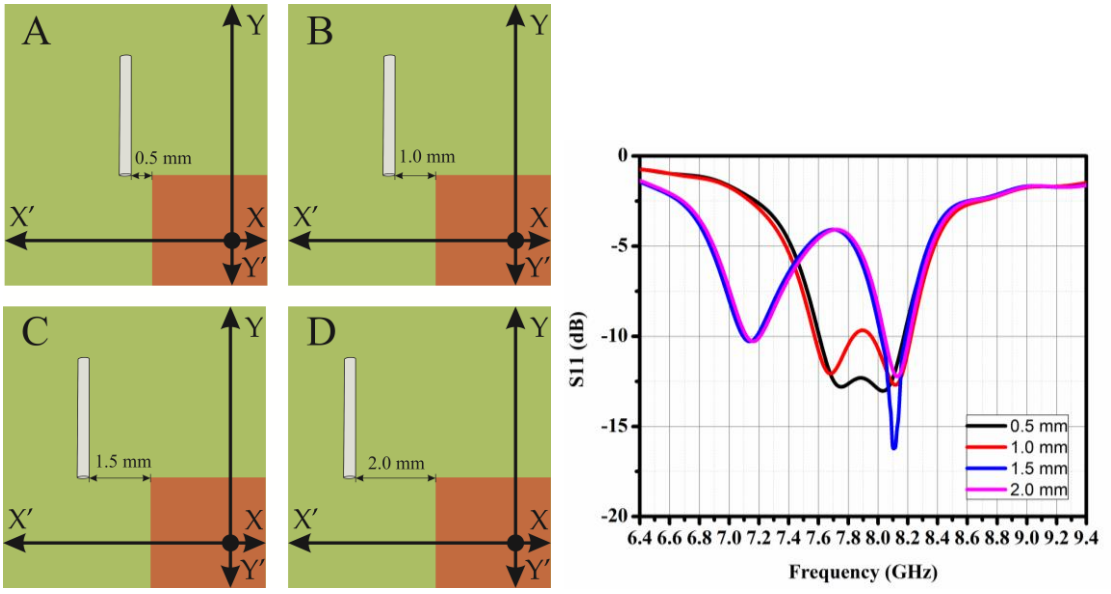

Figure 5.4 Optimization of channels position in X axis along with S11 plot

At first, the position of set A is optimized for stable S11 parameters. The process is started with considering a single element. The position of the element along the X axis is first optimized and initially it is placed 0.5 mm apart from the non-radiating

edge of the antenna patch. The spacing is then successively increased by a distance of 0.5 mm and the corresponding S11 parameters are simulated. Figure 5.4 shows the details of the optimization process.

From the S11 plots it is observed for a separation of 1.5 mm and above, the effect of the element is negligible on the antenna return loss parameter. Taking 1.5 mm as the separation between the radiator and the element further optimizations are carried out. Along the Y axis also the tubes are moved in a similar way to obtain suitable S11 value. The optimum distance is found to be 1mm and details are presented in Figure 5.5. The process is also repeated for the set B, C and D.

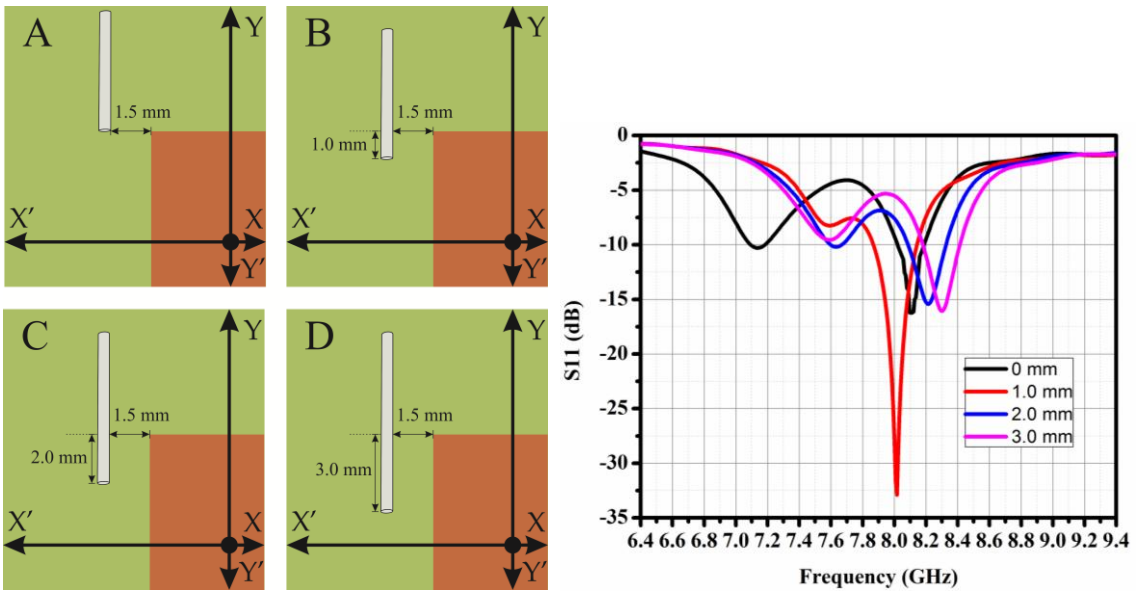

Figure 5.5 Optimization of channels position in Y axis along with S11 plot

Optimization of number of directing elements and inter channel spacing

Unlike, the PIN diode configuration, the liquid filled microchannels are used in pairs to form a single directing element and each of the sets contains two such pairs. The reason for pairing is the fact that on conducting simulation as well as experimental performance study it is found that the shift is more prominent when directing elements are in pairs, this could be because of lower conductivity of NaCl solution as compared to copper. The simulated result for single and paired channel is present in Figure 5.6.

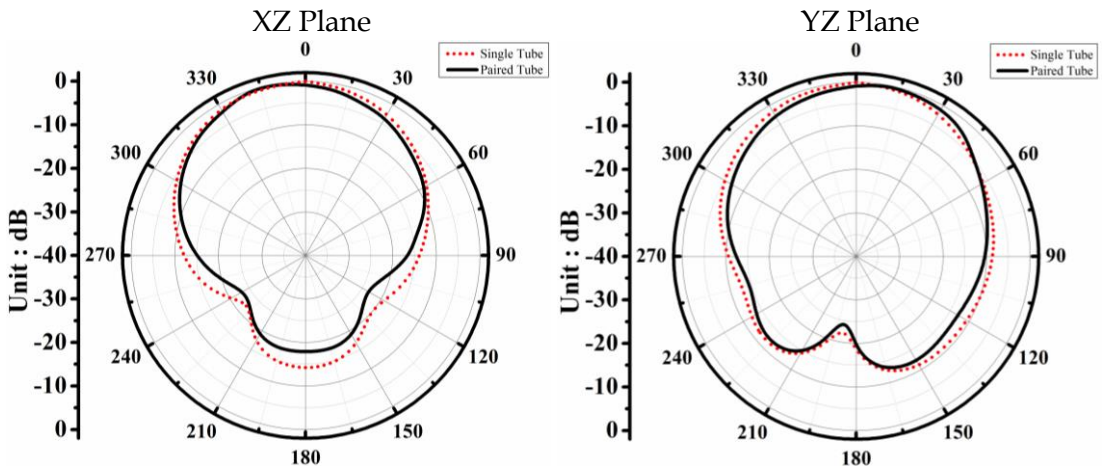

Figure 5.6 Simulated radiation pattern for single vs. paired channels. For single channel beam direction is 358˚ and 4˚ in XZ and YZ plane respectively. With paired element it is shifted to 352˚ and 10˚.

After finalizing the first element's position, a second element is added alongside. A separation of 1 mm gives the optimum results. In this work, two such pairs of channels are taken in each set for proof of concept. The number of elements can be further increase for larger beam coverage, however, to limit the design complexity only two elements per set is used. The optimized antenna dimensions are given in Table 5.1 and the final antenna is shown in Figure 5.7.

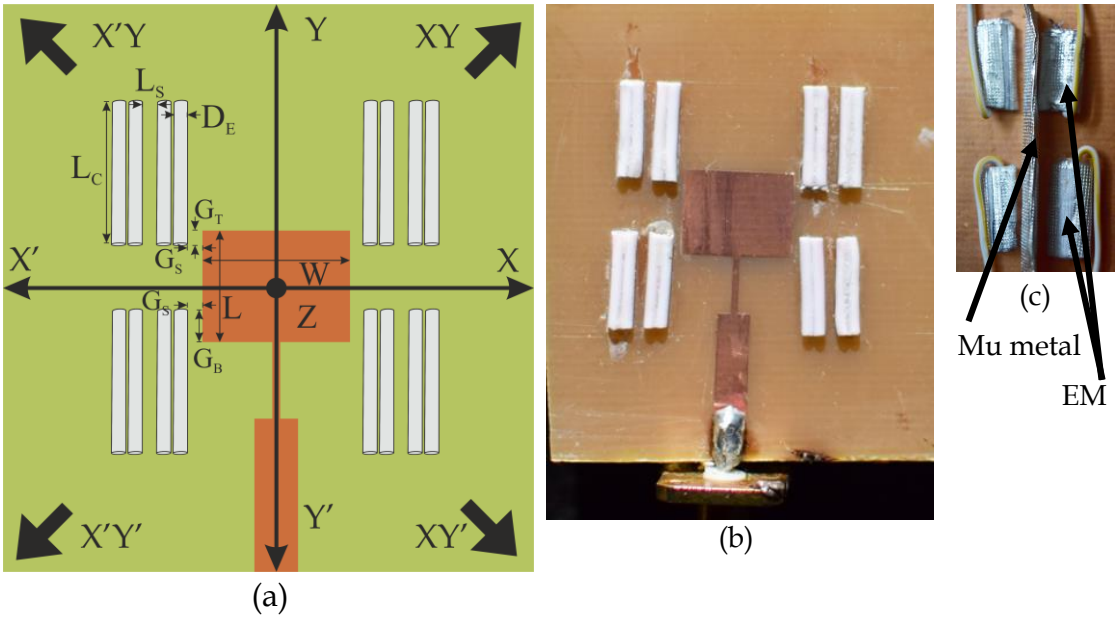

Figure 5.7 (a) Schematic diagram of the optimized antenna, (b) fabricated antenna and (c) magnified image of the backside of the antenna showing electromagnets (EM) covered and separated by mu metal

Table 5.1 Antenna design parameters

Parameter	L	W	L_C	L_S	D_E	G_S	G_T	G_B
Value (mm)	8.38	11.52	10.38	1	0.9	1	1.5	2

5.4 Reconfiguration of the antenna beam pattern

The prototype antenna is accessed for the pattern reconfiguration using the proposed contactless electromagnetically controlled tuning mechanism. Following sections discuss the implementation of the mechanism and operational performances of the antenna.

5.4.1 Implementation of the reconfiguration mechanism

Reconfiguration of the antenna beam is done by changing the state of the parasitic microfluidic channels. As mentioned in the previous section, the position of ferrofluid (FF) is toggled between the far end and the middle of each channel. Two electromagnets are used to provide necessary actuations to FF. Figure 5.8 shows the working of the fluidic antenna elements.

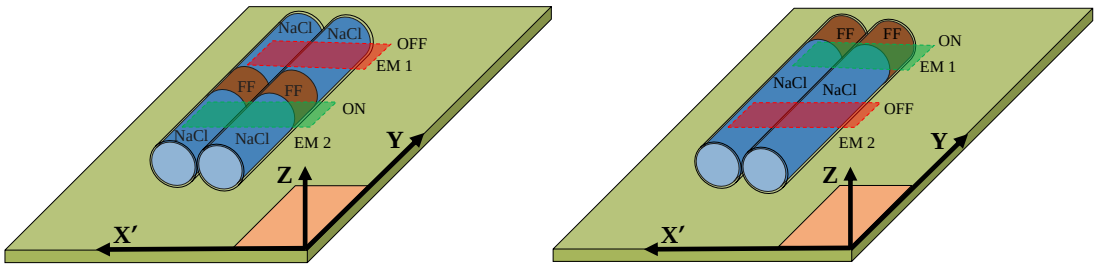

Figure 5.8 Illustration of the reconfiguration sequences. (a) EM 1 is OFF and EM 2 is ON, (b) EM 1 is ON and EM 2 is OFF. Shaded red and green colour rectangles shows the position of the EM at the back side of the antenna (ground plane).

In Figure 5.8 (a) electromagnet EM 2 is ON and FF is positioned at the center of the channel. At this condition, the NaCl solution splits into two parts and thus the channel does not has any beam directing capability and the condition is denoted as **0**. Secondly, EM 1 is switched ON (Figure 5.8 (b)) and FF shifts to the far end. Consequently, conductive NaCl acquires the necessary length and the channel serve as a directing element. The state is denoted by **1**. Details are presented in Table 5.2.

Table 5.2 Electromagnet switching with position of FF and switching state

EM 1	EM 2	FF Position	Switching State Term
OFF	ON	Middle	**0**
ON	OFF	Far End	**1**

5.4.2 Performance study of the beam reconfigurable antenna

The performance of the prototype antenna is tested experimentally along with simulations. First, the antenna is assessed for both return loss and radiation pattern placing ferrofluid solutions in the middle of the channels for all the elements.

At this stage, the fluidic channels do not act as director and the antenna beam pattern is similar to that of RMA (Figure 5.9).

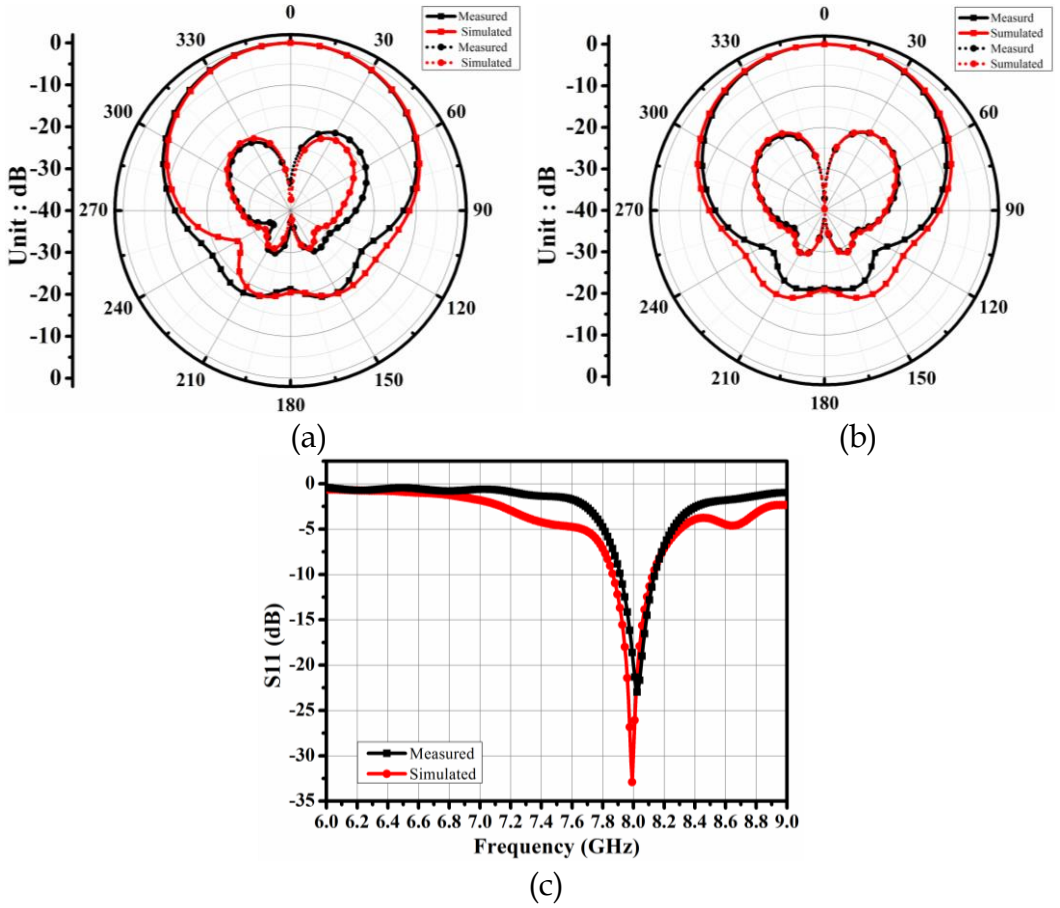

Figure 5.9 Measured and simulated (a) XZ plane, (b) YZ plane radiation patterns and (c) S11 parameters with all the directing elements in void state. Solid black and red line shows measured and simulated co-polar plots. Dotted black and red lines shows the corresponding cross-polar plots.

The beam is swept by controlling the state of the fluidic channels present at the four corners of the radiating patch. The sweeping is performed in two schemes similar to that present in Chapter III.

(i) Activating fluidic elements of a single set.

(ii) Activating fluidic elements of adjacent sets.

Activating fluidic elements of a single set

Liquids present in the channels of a single set are subjected to translational motion in this scheme. The position of FF is interchanged between two points as shown in Figure 5.8. The scheme is illustrated considering set A. At the beginning of the measurements FF is positioned in the middle of the tubes (State **0**) to make the antenna radiates in the broadside direction. The beam reconfiguration is carried out by sequentially changing the channel state to **1**. The activation sequence and corresponding pattern parameters are given in Table 5.3.

Table 5.3 Beam direction and beamwidth for sequence Sq 0 – Sq 2

Sequence	**FF position**		**Beam Direction XZ Plane (˚)**		**Beam Direction YZ Plane (˚)**		**Beamwidth XZ Plane (˚)**		**Beamwidth YZ Plane (˚)**	
	Ch_{A1}	**Ch_{A2}**	**Meas.**	**Simul.**	**Meas.**	**Simul.**	**Meas.**	**Simul.**	**Meas.**	**Simul.**
Sq 0	**0**	**0**	0	0	0	0	69.97	78.98	70.00	79.08
Sq 1	**1**	**0**	354	352	10	10	97.63	85.46	66.05	72.85
Sq 2	**1**	**1**	345	340	15	15	97.63	85.46	66.05	72.85

Meas. = Measured, Simul. = Simulated

For the sequence Sq 0 both the elements Ch_{A1} and Ch_{A2} are inactive and the beam pattern (Figure 5.9) resembles that of RMA. A shifting of ~ 10˚ from the broadside direction is observed for the sequence Sq 1 in both XZ and YZ plane and it is increased to ~ 15˚ for sequence Sq 2. The beam width of the patterns are fairly stable, it is around 90˚ ± 6˚ in XZ plane and 70˚ ± 8˚ in YZ plane. The patterns also exhibit lower cross-polarization levels. Co and Cross polar plots are shown in Figure 5.10.

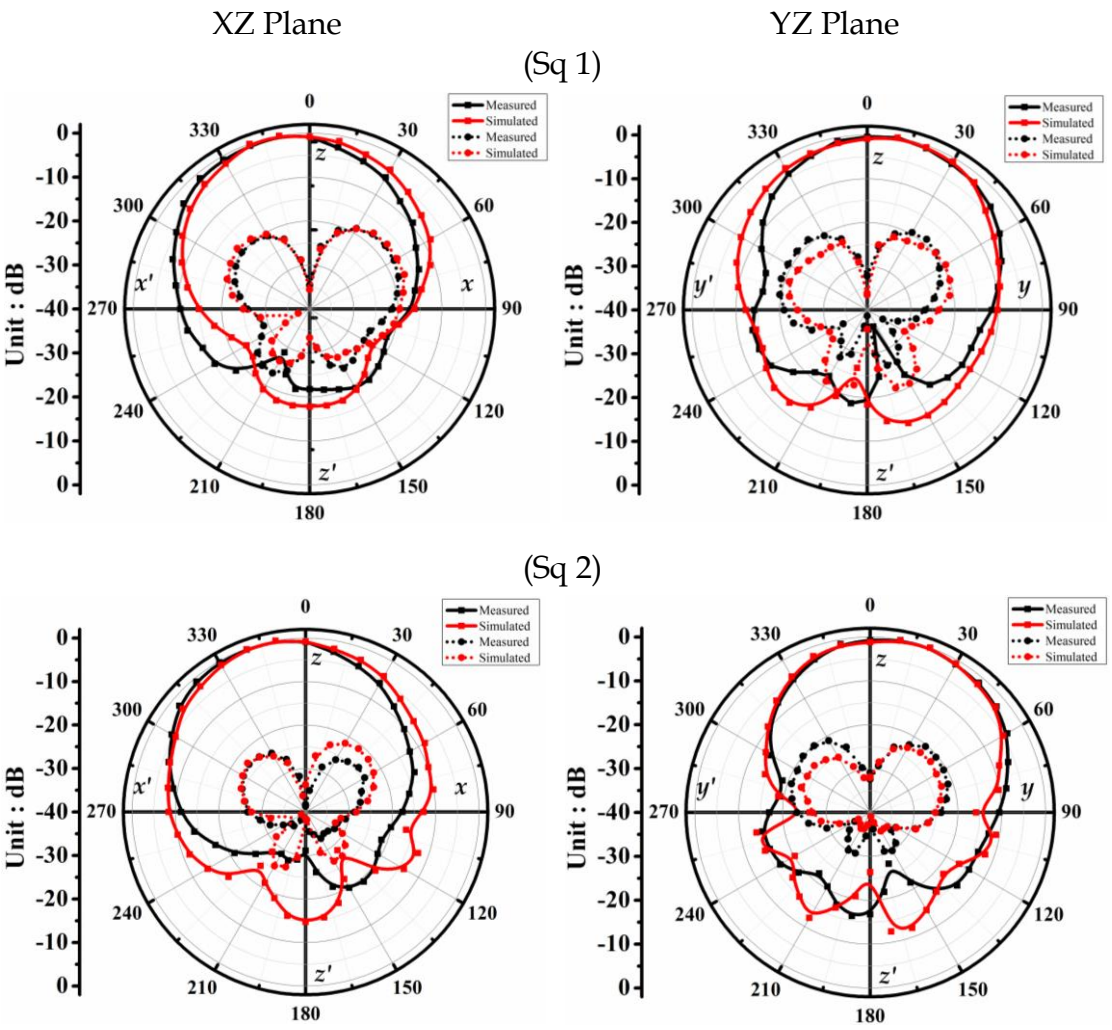

Figure 5.10 Radiation patterns in XZ and YZ planes for sequences Sq 1 and Sq 2. Solid black and red line shows measured and simulated co-polar plots. Dotted black and red lines shows the corresponding cross-polar plots.

The surface current distributions for the sequences are presented in Figure 5.11. In the Sq 0 current density is negligible in the parasitic elements as compared to the main antenna radiator. An increased current density is observed across the element Ch_{A1} for sequence Sq 1. This is because of the parasitic coupling between the channels and the antenna patch. Similarly, for Sq 2, the density spreads across the Ch_{A2} also. Figure 5.11 also contains simulated 3-dimensional plots showing the direction of beam shifting.

Activating fluidic elements of adjacent sets

The scheme describes the FF movements in two vicinal sets. In continuation with the previous scheme, directing elements of sets A and C are taken for discussion.

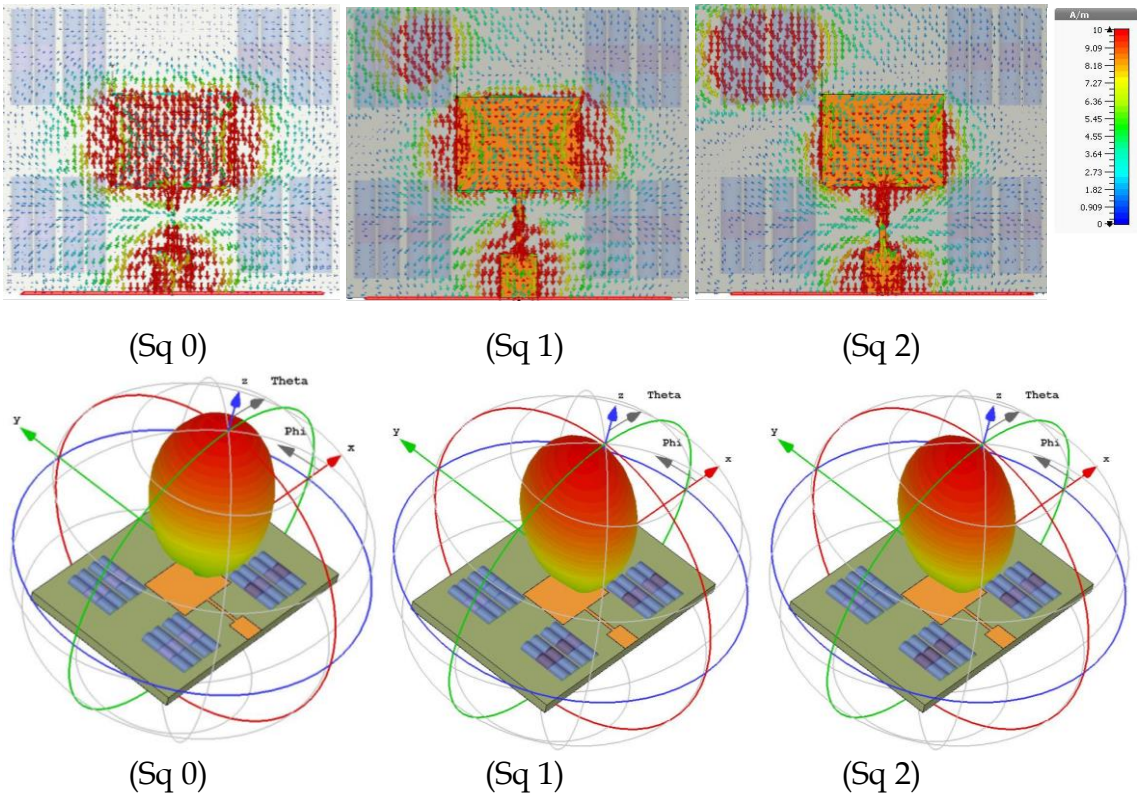

Figure 5.11 Surface current distribution and 3 – D radiation pattern plots for sequences given in Table 5.3.

Table 5.4 lists the combinations of activation sequences. Fluidic elements Ch_{A1} and Ch_{C1} are activated in sequence Sq 3 and due to the parasitic coupling the beam shifts to 350˚ in the X′ direction without any deviation in the YZ plane. A further declination is observed for Sq 4 with beam pointing at 330˚ in XZ plane. Out of all these elements Ch_{C2} is deactivated in Sq 5, the beam relocates to 355˚ in XZ plane and 20˚ in YZ plane. The corresponding beamwidths are listed in Table 5.4. The radiation pattern plots are presented in Figure 5.12.

Table 5.4 Beam direction and beamwidth for sequence Sq 3 – Sq 4

Sequence	FF position				Beam Direction XZ Plane (˚)		Beam Direction YZ Plane (˚)		Beamwidth XZ Plane (˚)		Beamwidth YZ Plane (˚)	
	Ch_{A1}	Ch_{A2}	Ch_{C1}	Ch_{C2}	Meas.	Simul.	Meas.	Simul.	Meas.	Simul.	Meas.	Simul.
Sq 3	**1**	**0**	**1**	**0**	350	355	0	0	69.97	78.98	70.00	79.08
Sq 4	**1**	**1**	**1**	**1**	335	335	0	0	99.00	99.00	75.44	75.44
Sq 5	**1**	**1**	**1**	**0**	355	355	20	20	84.56	84.56	62.12	62.12

Meas. = Measured, Simul. = Simulated

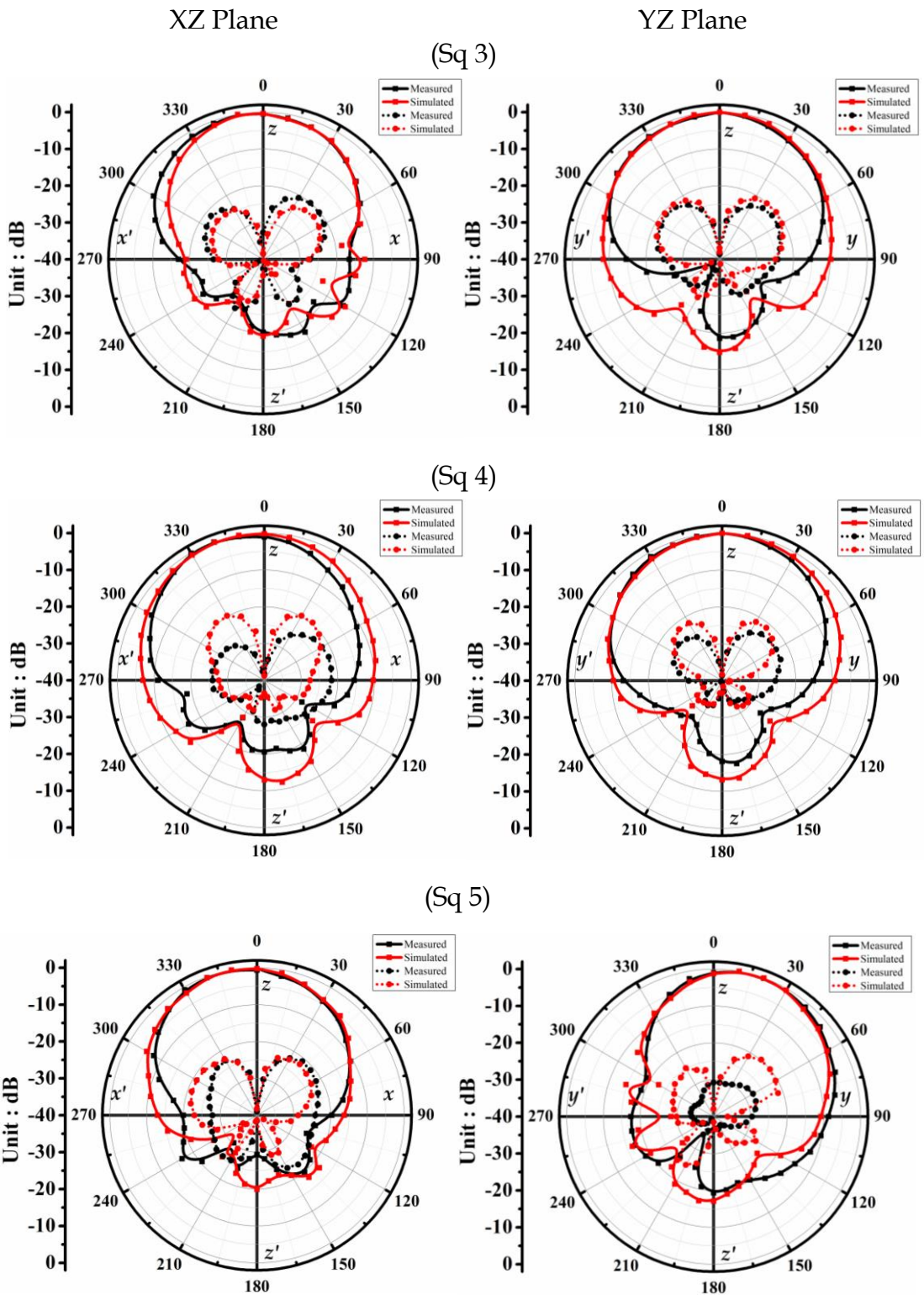

Figure 5.12 Radiation patterns in both XZ and YZ plane for sequences Sq 3 and Sq 5. Solid black and red line shows measured and simulated co-polar plots. Dotted black and red lines shows the corresponding cross-polar plots.

Figure 5.13 shows the current distribution plots for the sequences and similar to the Figure 5.11, increased current densities are observed across the activated elements.

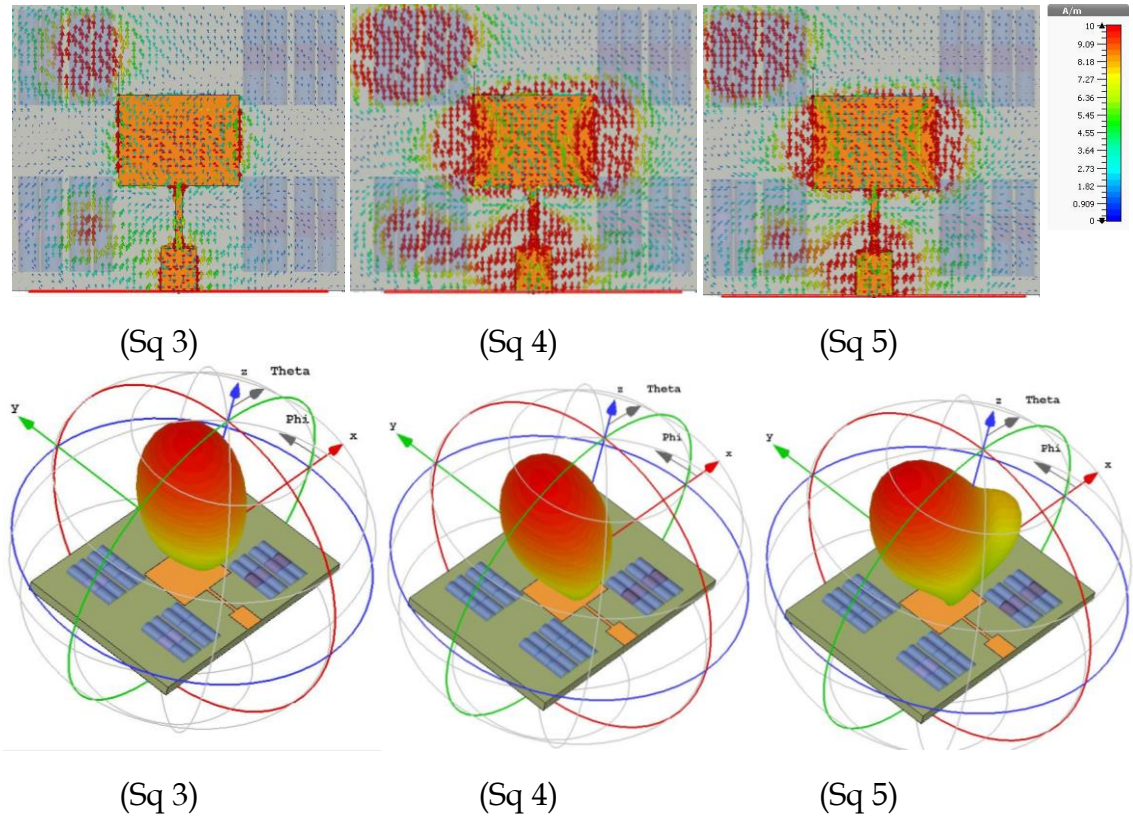

Figure 5.13 Surface current distribution and 3 – D radiation pattern plots for sequences given in Table 5.4.

The resonating behaviours of the antenna for the activation sequences are assessed by measuring the antenna return loss. The S11 plots given in Figure 5.14

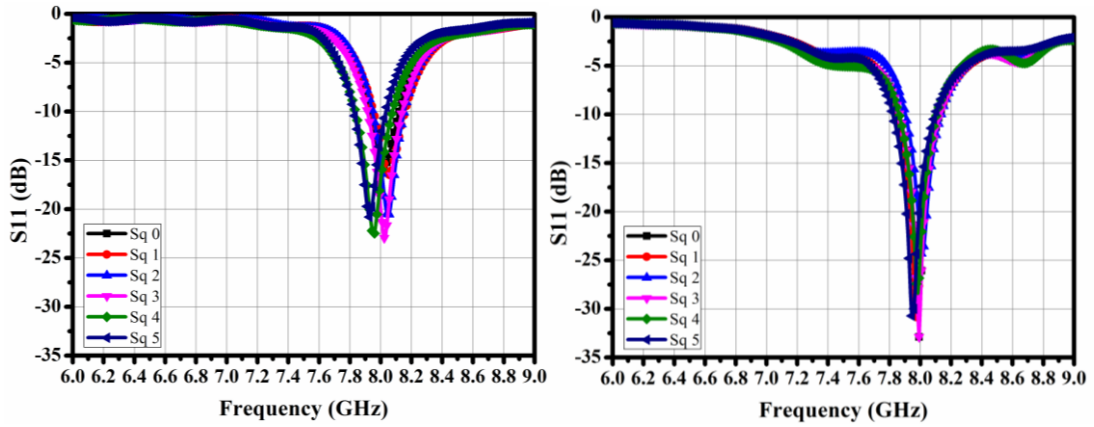

Figure 5.14 (a) Measured and (b) simulated S11 plots for sequences Sq 0 – Sq 5

exhibits fairly stable resonating frequency of the antenna at various reconfigured states. The antenna resonates within a frequency range of 0.10 GHz for all the reconfigured beam positions and maintains a – 10 dB bandwidth of around 0.20 GHz. The proposed antenna exhibits an average gain of 4.8 dBi and directivity of around 8.2 dB for all the swept beam directions. Details are listed in Table 5.5.

Table 5.5 Antenna performance parameters for the reconfigured sequences

Sequence	Frequency (GHz)	Bandwidth (MHz)	Directivity (dB)	Gain (dB)	Efficiency
Sq 0	7.92	180	8.4	5.2	62%
Sq 1	8.08	194	8.0	5.1	64%
Sq 2	8.04	200	8.2	4.8	59%
Sq 3	8.00	196	8.6	4.6	53%
Sq 4	7.96	192	8.3	4.4	53%
Sq 5	7.90	200	8.5	4.2	49%

Activation of directing elements in sets B, C and D shifts the beam in other directions. The beam can be reconfigured to 19 other directions by changing the combination in which elements are activated. However, due to the similarity in the results, plots are not presented in this chapter.

5.5 Discussion

The presented work offers a proximately controlled reconfiguration technique for steering of antenna beam pattern. Microfluidic channels form an array of directing elements, whose state can be toggled as per the requirements. The method advances over most of the reported liquid based tuning techniques [1, 5, 7, 9, 12, 15-18] as it does not require any bulky pump mechanism and complex network of connecting pipelines. This method exploits the conducting property of polar solutions for directing the beam, thus reducing the risk of being exposed to hazardous toxic metals like Mercury or working with the temperature limit of Galinstan.

Controlled through a pair of electromagnets attached to each directing elements, multi-stepped reconfigurations are achieved. The beam can be shifted to 19 different directions and the antenna preserves the consistency of its resonating

frequency for all the reconfigured beam patterns around 8 GHz. Directivity and gain are also fairly stable with values 8.3 ± 0.3 dB and 4.7 ± 0.5 dBi respectively.

The works presented in Chapter III and Chapter V shows two different technique to realize beam reconfigurability in a planar microstrip patch antenna. The technique presented in Chapter V is a proximity controlled, contactless method for steering of antenna beam pattern. The proposed electromagnetically controlled microfluidic reconfiguration technique effectively converts a standard rectangular patch antenna into a beam scanning antenna. The modus operandi of the system demonstrates the features of a multi radiator antenna in a single driven element antenna. The contactless technique of reconfiguration also reduces auxiliary bias units as used in electrical /optical switching systems. For the proximity controlled technique, directivity is higher than the electrical technique presented in Chapter III. However, due to the low conductivity value of the liquid used efficiency is less than the electrical reconfiguration technique.

References

[1] Rodrigo, D., Jofre, L., and Cetiner, B.A. Circular Beam-Steering Reconfigurable Antenna With Liquid Metal Parasitics. *IEEE Transactions on Antennas and Propagation,* 60(4):1796-1802, 2012. DOI:10.1109/TAP.2012.2186235

[2] Entesari, K., and Saghati, A.P. Fluidics in Microwave Components. *IEEE Microwave Magazine,* 17(6):50-75, 2016. DOI:10.1109/MMM.2016.2538513

[3] Huff, G.H., Rolando, D.L., Walters, P., and McDonald, J. A Frequency Reconfigurable Dielectric Resonator Antenna Using Colloidal Dispersions. *IEEE Antennas and Wireless Propagation Letters,* 9:288-290, 2010. DOI:10.1109/LAWP.2010.2046613

[4] Khan, M.R., Hayes, G.J., So, J.-H., Lazzi, G., and Dickey, M.D. A frequency shifting liquid metal antenna with pressure responsiveness. *Applied Physics Letters,* 99(1):013501, 2011. DOI:10.1063/1.3603961

[5] Kim, D., Pierce, R.G., Henderson, R., Doo, S.J., Yoo, K., and Lee, J.-B. Liquid metal actuation-based reversible frequency tunable monopole antenna. *Applied Physics Letters,* 105(23):234104, 2014. DOI:10.1063/1.4903882

[6] King, A.J., Patrick, J.F., Sottos, N.R., White, S.R., Huff, G.H., and Bernhard, J.T. Microfluidically Switched Frequency-Reconfigurable Slot Antennas. *IEEE Antennas and Wireless Propagation Letters,* 12:828-831, 2013. DOI:10.1109/LAWP.2013.2270940

[7] Saghati, A.P., Batra, J., Kameoka, J., and Entesari, K. A microfluidically-tuned dual-band slot antenna. in *2014 IEEE Antennas and Propagation Society International Symposium (APSURSI)*, 1244-1245, 2014.

[8] Wang, M., Trlica, C., Khan, M.R., Dickey, M.D., and Adams, J.J. A reconfigurable liquid metal antenna driven by electrochemically controlled capillarity. *Journal of Applied Physics,* 117(19):194901, 2015. DOI:10.1063/1.4919605

[9] Bhattacharjee, T., Jiang, H., and Behdad, N. Fluidic beam steering in parasitically coupled patch antenna arrays. *Electronics Letters,* 51(16):1229-1231, 2015. DOI:10.1049/el.2015.1908

[10] Hu, W., Ismail, M.Y., Cahill, R., Encinar, J.A., Fusco, V.F., Gamble, H.S., Linton, D., Dickie, R., Grant, N., and Rea, S.P. Liquid-crystal-based reflectarray antenna with electronically switchable monopulse patterns. *Electronics Letters,* 43(14):1, 2007. DOI:10.1049/el:20071098

[11] Bildik, S., Dieter, S., Fritzsch, C., Frei, M., Fischer, C., Menzel, W., and Jakoby, R. Reconfigurable liquid crystal reflectarray with extended tunable phase range. in *2011 41st European Microwave Conference*, 1292-1295, 2011.

[12] Morishita, A.M., Kitamura, C.K.Y., Ohta, A.T., and Shiroma, W.A. A Liquid-Metal Monopole Array With Tunable Frequency, Gain, and Beam Steering. *IEEE Antennas and Wireless Propagation Letters,* 12:1388-1391, 2013. DOI:10.1109/LAWP.2013.2286544

[13] Huang, J., and Densmore, A.C. Microstrip Yagi array antenna for mobile satellite vehicle application. *IEEE Transactions on Antennas and Propagation,* 39(7):1024-1030, 1991. DOI:10.1109/8.86924

[14] Balanis, C.A. *Antenna theory: analysis and design*. John Wiley & Sons. 2016.

[15] Wang, C., Yeo, J.C., Chu, H., Lim, C.T., and Guo, Y. Design of a Reconfigurable Patch Antenna Using the Movement of Liquid Metal. *IEEE Antennas and Wireless Propagation Letters,* 17(6):974-977, 2018. DOI:10.1109/LAWP.2018.2827404

[16] Konca, M., and Warr, P.A. A Frequency-Reconfigurable Antenna Architecture Using Dielectric Fluids. *IEEE Transactions on Antennas and Propagation,* 63(12):5280-5286, 2015. DOI:10.1109/TAP.2015.2490243

[17] Bhattacharjee, T., Jiang, H., and Behdad, N. A Fluidically Tunable, Dual-Band Patch Antenna With Closely Spaced Bands of Operation. *IEEE*

Antennas and Wireless Propagation Letters, 15:118-121, 2016. DOI:10.1109/LAWP.2015.2432575

[18] Chen, Z., and Wong, H. Liquid Dielectric Resonator Antenna With Circular Polarization Reconfigurability. *IEEE Transactions on Antennas and Propagation,* 66(1):444-449, 2018. DOI:10.1109/TAP.2017.2762005